MIDAS – THE MICRO-IMAGING DUST ANALYSIS SYSTEM FOR THE ROSETTA MISSION

W. RIEDLER[1], K. TORKAR[1,*], H. JESZENSZKY[1], J. ROMSTEDT[2], H. ST. C. ALLEYNE[12], H. ARENDS[2], W. BARTH[4], J. V. D. BIEZEN[2], B. BUTLER[2], P. EHRENFREUND[6], M. FEHRINGER[2], G. FREMUTH[1], J. GAVIRA[2], O. HAVNES[9], E. K. JESSBERGER[5], R. KASSING[4], W. KLÖCK[10], C. KOEBERL[11], A. C. LEVASSEUR-REGOURD[7], M. MAURETTE[8], F. RÜDENAUER[3], R. SCHMIDT[2], G. STANGL[13], M. STELLER[1] and I. WEBER[5]

[1]*Institut für Weltraumforschung, Österreichische Akademie der Wissenschaften, Schmiedlstrasse 6, 8042 Graz, Austria*

[2]*Science Directorate, ESA/ESTEC, 2200 AG Noordwijk, The Netherlands*

[3]*ARC Seibersdorf research GmbH, 2444 Seibersdorf, Austria*

[4]*Institut für Technische Physik, Universität Gesamthochschule Kassel, 34109 Kassel, Germany*

[5]*Institut für Planetologie, Westfälische Wilhelms-Universität Münster, 48149 Münster, Germany*

[6]*Sterrewacht Leiden, 2300 RA Leiden, The Netherlands*

[7]*Université Paris 6/Aéronomie CNRS, 91371 Verrières, France*

[8]*Astrophysique du Solide, C.S.N.S.M., 91405 Orsay-Campus, France*

[9]*Auroral Observatory, University of Tromsø, 9037 Tromsø, Norway*

[10]*Röntgenanalytik Messtechnik GmbH, 65232 Taunusstein, Germany*

[11]*Center for Earth Sciences, Universität Wien, 1090 Vienna, Austria*

[12]*University of Sheffield, Sheffield S1 4DU, United Kingdom*

[13]*Institut für Sensor- und Aktuatorsysteme, Technische Universität Wien, 1040 Vienna, Austria*

(*Author for correspondence: E-mail: klaus.torkar@oeaw.ac.at)

(Received 17 February 2006; Accepted in final form 27 September 2006)

Abstract. The International Rosetta Mission is set for a rendezvous with Comet 67 P/Churyumov-Gerasimenko in 2014. On its 10 year journey to the comet, the spacecraft will also perform a fly-by of the two asteroids Stein and Lutetia in 2008 and 2010, respectively. The mission goal is to study the origin of comets, the relationship between cometary and interstellar material and its implications with regard to the origin of the Solar System. Measurements will be performed that shed light into the development of cometary activity and the processes in the surface layer of the nucleus and the inner coma.

The Micro-Imaging Dust Analysis System (MIDAS) instrument is an essential element of Rosetta's scientific payload. It will provide 3D images and statistical parameters of pristine cometary particles in the nm-μm range from Comet 67P/Churyumov-Gerasimenko. According to cometary dust models and experience gained from the Giotto and Vega missions to 1P/Halley, there appears to be an abundance of particles in this size range, which also covers the building blocks of pristine interplanetary dust particles. The dust collector of MIDAS will point at the comet and collect particles drifting outwards from the nucleus surface. MIDAS is based on an Atomic Force Microscope (AFM), a type of scanning microprobe able to image small structures in 3D. AFM images provide morphological and statistical information on the dust population, including texture, shape, size and flux. Although the AFM uses proven laboratory technology, MIDAS is its first such application in space. This paper describes the scientific objectives and background, the technical implementation and the capabilities of MIDAS as they stand after the commissioning of the flight instrument, and the implications for cometary measurements.

Space Science Reviews (2007) 128: 869–904
DOI: 10.1007/s11214-006-9040-y

Keywords: Rosetta, atomic force microscope, comet, coma, dust, 67P/Churyumov-Gerasimenko

1. Introduction

1.1. Overview

Due to the importance of measuring the dust emitted from the comet nucleus, one of the essential instruments for the Rosetta mission is the Micro-Imaging Dust Analysis System (MIDAS), dedicated to the microtextural and statistical analysis of cometary dust particles. The instrument described in this paper is based on the technique of scanning force microscopy, which has made rapid progress in recent years. The instrument will for the first time image interplanetary and pristine cometary particles in the nm-μm range in 3D. It will also provide morphological and statistical information on the dust population, including texture, shape, size and flux. This paper describes the MIDAS scientific objectives dedicated to the collection of very small particles and the characterisation of materials by atomic force microscopy. Finally, it presents the technical solutions adopted for this inaugural implementation of the technique on a space mission and the capabilities as confirmed in the post-launch commissioning. To study the nature of cometary material is crucial and will provide important constraints on the true nature of the early solar nebula.

1.2. Scientific Background

Comets are believed to have formed in cool and distant regions of the early Solar System. Thus, cometary matter might preserve some of the original signatures of the interstellar materials that build up planetary systems (Irvine and Lunine, 2004; Ehrenfreund *et al.*, 2004). In a simplified view, comets are made of silicates ($\sim$25%), organic refractory material ($\sim$25%), small carbonaceous molecules ($\sim$10%), and $\sim$50% water ice with small admixtures of other ice species (Greenberg, 1998). Once a comet is transferred from its remote storage place in the Kuiper belt or the Oort cloud, respectively, into a highly elliptical orbit around the Sun, the previously rather quiet body begins to exhibit physical activity. Temperatures increase on its way towards the Sun, and the icy substances begin to sublimate. The released gases drag a large amount of solid μm- and sub-μm-sized particles into space. Molecular ices and the gases released upon sublimation, silicate dust and solid state carbonaceous materials are the major components of dusty cometary comae which can be studied by astronomical observations and with the aid of laboratory and numerical simulations (Rodgers and Charnley, 2004; Hanner and Bradley, 2004; Colangeli *et al.*, 2004; Kolokolova *et al.*, 2004). Ground-based and space borne spectroscopic analyses in the last decades have added substantial information about the composition of

comets. From radio spectroscopic observations of comets, more than 22 molecules, radicals and ions, plus several isotopologues, were detected, predominantly in the comae of comets C/1996 B2 (Hyakutake) and C/1995 O1 (Hale-Bopp) (Crovisier *et al.*, 2004). A comparison between Infrared spectra of comets and laboratory studies of particles collected in the Earth environment (so-called IDPs) and presumed to be of cometary origin shows that silicates in comets are dominated by two minerals – olivine and pyroxene, and are identified in two forms – amorphous and crystalline (Hanner and Bradley, 2004; Colangeli *et al.*, 2004). Crystalline silicates in comets are of probable nebular origin and are revealed by the sharp resonances in cometary 10 μm spectra (e.g. Hanner and Bradley, 2004). The appearance of Mg-rich crystalline silicates in some comets and the scarcity of crystalline silicates in the ISM indicates cometary crystalline silicates are grains that condensed at high temperatures ($\sim$1400 K, Hanner and Bradley, 2004) or were annealed from amorphous silicates at somewhat lower temperatures ($>$900 K, Hallenbeck *et al.*, 2000; Hanner and Bradley, 2004) in the solar nebula. Annealing also may have occurred in shocks in the nebula in the 5–10 AU region, producing local enhancements in the crystalline concentration (Harker and Desch, 2002). Recent data from the Stardust mission to Comet 81P/Wild-2 have shown the presence of mineral crystals such as forsterite, pyroxene, anorthosite, spinel, and titanium nitride, which all formed at moderately high to extremely high temperatures. These minerals must have formed at temperatures of at least 1400 K, especially some particles resembling the so-called calcium-aluminum inclusions (CAIs) known from meteorites (e.g., Kerr, 2006; McKeegan *et al.*, 2006; Zolensky *et al.*, 2006). Thus at least some comets contain material from the inner and outer reaches of the solar system.

Complementary to information about the composition, information about the physical properties of cometary dust is provided by in-situ (impacts, light scattering) and remote observations, together with numerical and laboratory simulations (Kolokolova *et al.*, 2004). In-situ studies suggest that cometary dust particles have low densities – about 100 kg m^{-3} for comet 1P/Halley (Fulle *et al.*, 2000) – and consist of easily fragmenting aggregates (Clark *et al.*, 2004). These studies, as well as the enrichment of deuterium compared to hydrogen observed in some IDPs, are in excellent agreement with the Greenberg (1982) hypothesis of porous aggregates of partly photo-chemically processed submicrometer-sized interstellar dust grains (e.g., Levasseur-Regourd *et al.*, 2006). From the numerous polarimetric measurements available for comet C/1995 O1 Hale-Bopp, a power law size distribution with an index of (-3), radii of about 0.1 μm for the smallest grains and equivalent radii of about 20 μm for the biggest ones has been derived (Lasue and Levasseur-Regourd, 2006). For less active periodic comets, the power law index could be of about -2.5 or even less negative.

Comet 67P/Churyumov-Gerasimenko was discovered in 1969 and has been observed from Earth on six approaches to the Sun between 1969 and 2002. It is unusually active for a short period object and is classified as a dusty comet. The

peak dust production rate in 2002/03 was estimated at approximately 60 kg per second, although values as high as 220 kg per second were reported in 1982/83. The gas to dust emission ratio is approximately 2. HST's images showed that the nucleus measures five by three kilometres and has an ellipsoidal shape. The comet rotates once in approximately 12 hours. Recently a thermal evolution model of 67P/Churyumov-Gerasimenko has been computed by Di Sanctis *et al*. (2005) and compositional and physical results have been reported by Schleicher (2006). The evolution of the activity and composition of the coma of ROSETTA target comet 67P/Churyumov-Gerasimenko was studied along its post perihelion orbit from 2.29 AU to 3.22 AU (Schulz *et al*., 2004).

Cometary nuclei are highly porous agglomerations of grains of ice and dust and they appear stratified in density, porosity, ice phases and strength (Prialnik *et al*., 2004). Cometary gases and dust particles observed in cometary comae originate from the material of the nucleus and offer insight into the nucleus composition. Cometary material was analysed in situ for the first time in 1986. The time-of-flight mass spectrometers aboard the Vega and Giotto spacecraft provided information on the chemical composition of collected particles (e.g. Jessberger *et al*., 1988). A close look at the rock-forming elements (Jessberger, 1999) showed that a high percentage of Halley's dust consists mainly of Mg-rich silicates and to a lesser extent of Fe-sulphides and Fe-metal (Schulze *et al*., 1997). Halley's Fe/Mg ratio is 0.52 and the solar value is 0.84 (Jessberger *et al*., 1988). However, only 30% of the Fe is in silicates while 70% is in FeS and Fe grains. Halley's iron grains are highly reduced, as there is $<1\%$ FeO. This is also characteristic of the iron within GEMS (glass with embedded metal and sulphides; Messenger *et al*., 2003; Hanner and Bradley, 2004) in chondritic porous interplanetary dust particles (CP IDPs) where it exists as nanophase Fe or FeS and where the nanophase Fe has been attributed to ion bombardment in the interstellar medium (e.g., Bradley *et al*., 1999; Wooden, 2002). Remote measurements (e.g. Min *et al*., 2005) and returned cometary material by the Stardust mission (http://stardust.jpl.nasa.gov/home/index.html) reveals a significant amount of crystalline material in the dust coma of a comet. If the crystallinity is expressed in idiomorphic or hypidiomorphic shapes it will be possible to image these grains in the sub-μm size range.

Cometary carbon grains were claimed by Fomenkova and Chang (1996) to be predominant among the smaller particle population. These authors estimated the particle mass at 10^{-15} to 10^{-17} g, which corresponds to a radius of 0.01 to 0.5 μm and found a uniform distribution in Halley's neighbourhood. Since no correlation has been found to any other groups of particles or with respect to spatial distribution, it was concluded that these grains are of primary origin rather than a decay product of larger particles (Fomenkova and Chang, 1993). In contrast, from the dust mass spectrometer measurements at comet Halley it was found that silicate and carbonaceous components are mixed down to the finest scale. For the 0.1–1 micron size range Lawler and Brownlee (1992) derived from detailed analysis of the spectra that no particles with pure C, H, O, N element composition were detected. The

particle sizes for which size information is paired with chemistry range from 0.02 to 2 micrometer (Mass *et al.*, 1989).

Laboratory studies of CP IDPs indicated their cometary origin (Bradley, 1988; Hanner and Bradley, 2004). CP IDPs are aggregates of crystalline and amorphous silicates. They contain the so-called GEMS in a matrix of carbonaceous materials. The non-destructive storage of such fragile material requires a site offering extremely low geological activity. This clearly points towards a cometary source.

Pristine cometary material is subject to various ageing processes (Meech, 1991). It is highly likely that different materials will be observed at different times during the mission, and they could be correlated to the layered structure of the nucleus where the dust jets originate. It might be possible to distinguish between material that is released from the hard crust that covers every comet (Grün *et al.*, 1991) and fresh material from the interior. The Deep Impact mission has actually shown that the dust released by the impact from the subsurface after the impact consisted of very small grains and aggregates thereof (A'Hearn *et al.*, 2005) and that the bulk density of the nucleus is very low, of about $350 \pm 25\,\mathrm{kg\,m^{-3}}$ (A'Hearn, personal communication). The fresh material might still contain the interstellar grain size distribution. Hong and Greenberg (1980) suggest interstellar grains of a very complex composition. The different building units consist of silicates, organic materials and ices in the size range 0.01–0.2 μm. It is clearly within the capabilities of MIDAS to identify single components, fragments and whole grain assemblages if they are present in the cometary coma.

The Short Wavelength Spectrometer on ESA's Infrared Space Observatory (ISO) detected crystalline silicates at many different places in the Universe. These comprise young and evolved stars as well as planetary nebulae. One of ISO's surprising discoveries was the detection of crystalline silicates in Comet Hale-Bopp, in particular Mg-rich olivine (Crovisier *et al.*, 1997). Laboratory measurements confirmed that Mg-rich members of the olivine and pyroxene mineral groups were detected by ISO in an oxygen-rich circumstellar environment (Jäger *et al.*, 1998). Also, the grain size of cometary matter could be addressed by ground-based IR spectrophotometry that suggests a grain size of about 3 μm for silicatic components from Comet Tabur (Harker *et al.*, 1998).

Although the discussion about the specific origin(s) of IDPs is not yet closed, certain findings strongly suggest that some of the constitutents (e.g. GEMS) of certain types of IDPs have an origin in the early solar nebula. This suggests comets as the parent bodies, where they have been stored for the last 4560 million years. Bradley *et al.* (1983) identified enstatite whiskers and platelets in one group of IDPs. The unique crystal morphology such as rods, platelets, ribbons and their microstructures (e.g. stacking faults) led them to suggest that the particles may have formed either in the solar nebula or in a pre-solar environment. However, these crystals are very rare in extraterrestrial materials. Nevertheless, they are very characteristic if found from a comet.

2. Scientific Objectives

The challenge of counting and imaging the fresh cometary material calls for a unique tool – such as the MIDAS experiment. It is specialised on imaging cometary dust particles and their microstructure. The instrument carries 61 specially prepared target surfaces which will be sequentially exposed to the dust flux from the comet. After exposure, one or more images of each dust-loaded target will be produced. The area size of the images can be varied over a large range. The large overview images provide statistical data on the number of collected particles and reveal the locations of particles of particular interest. The instrument can then zoom in precisely on these particles, providing high-resolution images down to the nm level. The data analysis covers dust counting, imaging and characterisation. From the number of captured particles, the particle size and dust flux density distribution integrated over the collecting period can be deduced. The instrument's high-resolution capability reaches the smallest grain-size range ever observed, beyond any other Rosetta instrument. MIDAS is thus well-placed to complement other dust experiments, such as GIADA (Colangeli *et al*., this volume) and COSIMA (Kissel *et al*., this volume).

The following example demonstrates how distinctive features appear under the Atomic Force Microscope (AFM), the measurement technique applied in MIDAS. Figure 1 shows an AFM image of a $5 \times 5\ \mu$m scan area on a cosmic spherule. The overall surface is extremely smooth. A large number of tiny subparticles are attached to it. The smallest visible grains have a diameter of <20 nm. Within that order of magnitude, four different morphologies (arrowed) can be distinguished: (1) round; (2) elongated; (3) flat, platy individuals; (4) particle agglomerates. Furthermore, strict linear surface features suggest an internal structure different from the surface but imprinting it.

The measurements by the MIDAS instrument will address many of the questions related to cometary dust. In particular, the MIDAS instrument can measure and address the following qualities of the collected dust grains:

- 3D images of single particles;
- Images of the textural complexity of particle aggregates;
- Identification of crystalline material if idiomorphic or hypidiomorphic shapes are developed;
- Identification of sub-features on clean surfaces which provides insight into the growth conditions (e.g. twinning defects) and/or storage environment (e.g. dissolution marks);
- Statistical evaluation of the particles according to size, volume and shape;
- Variation of particle fluxes between individual exposures of the collector unit on time scales of hours;
- Four out of the sixteen sensors are capable to detect a magnetic gradient between sensor and sample and allow the identification of ferromagnetic minerals or the visualisation of the internal magnetic structure of a grain.

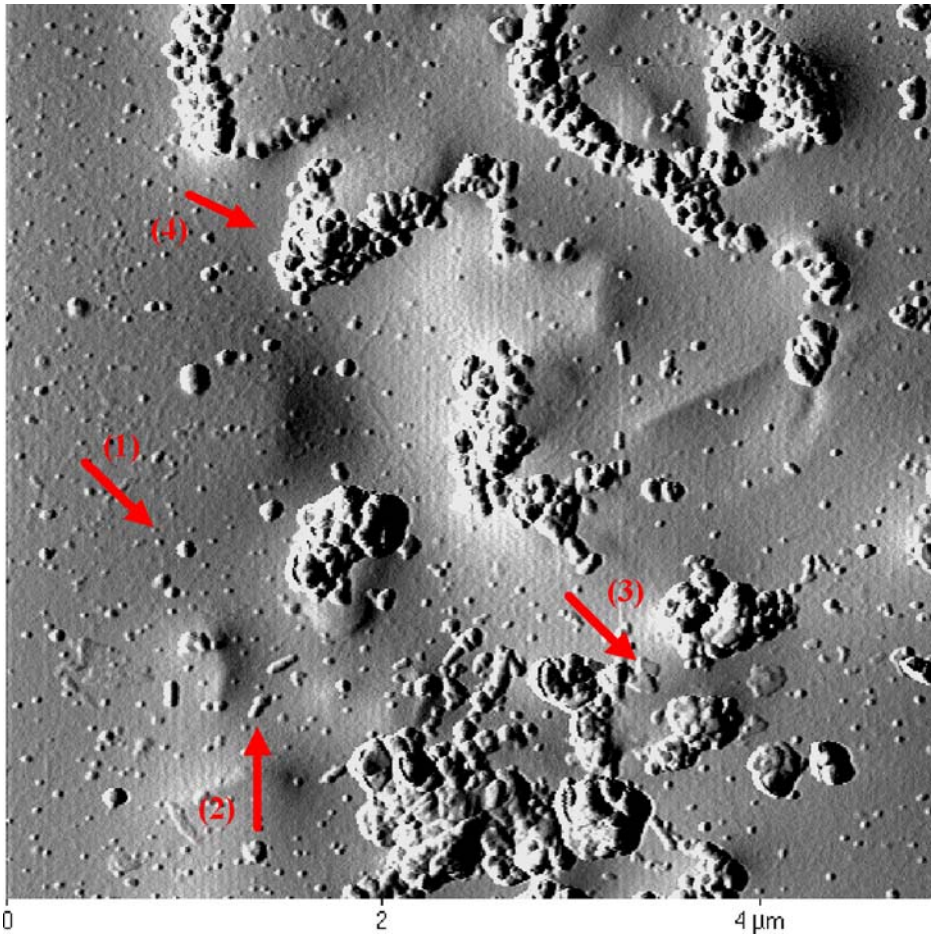

Figure 1. An AFM image of a cosmic spherule. Tiny individual objects are smaller than 20 nm. The arrows point towards distinctive objects (see text).

3. Dust Flux and Exposure Times

The design and operations planning of MIDAS requires a good understanding of the ambient dust flux and particle size distribution. ESA's dust model of Comet Wirtanen (Müller *et al.*, 1998) has been used for the initial design of a measurement strategy. The model is based on optical observations of the comet and extrapolations from data acquired by Giotto near Comet Halley, and has been used for the following estimations as a proxy for Churyumov-Gerasimenko. Agarwal *et al.* (2004) have applied the ESA Cometary Environment Model to the new Rosetta target, concluding for the insolation-driven case the dust density at two nucleus radii above the subsolar point of 67P/C-G is smaller by a factor of 3–5 than in the

coma of P/Wirtanen, but in the presence of a jet, the highest dust density is twice as high as for P/Wirtanen with insolation-driven activity. The terminal velocities of dust grains in the homogeneous case are less than those of P/Wirtanen, whereas in a jet they would be higher. We conclude that the model numbers previously obtained for P/Wirtanen would still serve as a good approximation of the average conditions observed by Rosetta. According to the ESA model for P/Wirtanen, the differential number flux per size decade of 'normal' dust grains in the mass range already previously identified near Halley can be well approximated by a power law in the size range of interest for MIDAS (grain radii $<2\,\mu$m). There are speculations (e.g. Fomenkova and Mendis, 1992) about the existence of a coma population of 'very small grains' (VSG, m $<10^{-21}$ kg), that escaped positive identification by Giotto, the only in situ mission to a comet so far. These grains are not considered in ESA's dust model. Figure 2 shows the exposure time required to collect 100 'normal' grains per decade size range on a $100 \times 100\,\mu$m collection area at 1 AU solar distance, calculated from the baseline number flux distribution together with the upper and lower limits following from ESA's model. Also shown in the figure are the power law approximation and the estimates given in the original MIDAS proposal, which over-estimate exposure times by 15–25%. Scaling factors have to be applied for other heliocentric distances of the comet and distances to the nucleus. Rüdenauer (1998) has combined several estimates into a numerical formula

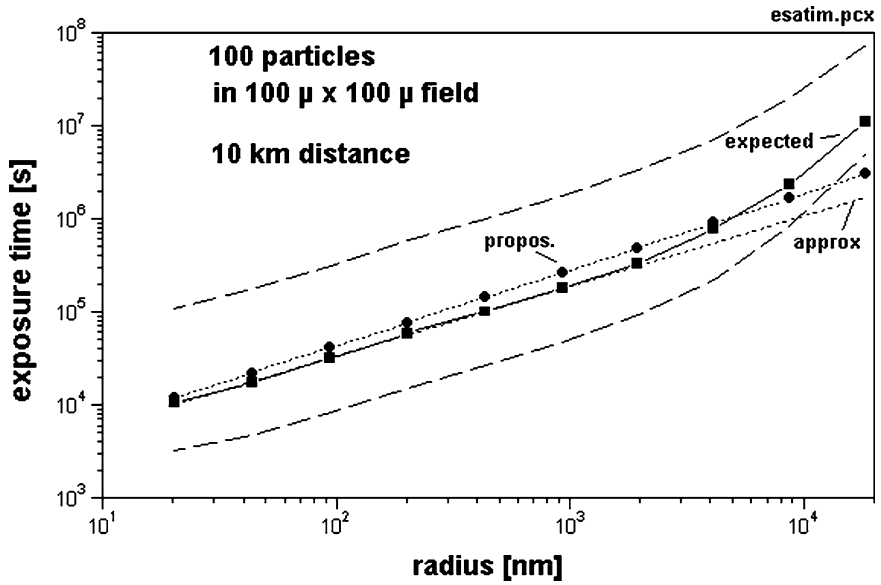

Figure 2. Exposure time required to collect 100 grains in respective decade size ranges at 1 AU solar distance. Squares and dashed lines are from ESA's figures; circles are from the MIDAS proposal; dotted lines are power approximations.

Equation (1) for the dust number flux, F_{nd} (grain m^{-2} s^{-1}), for a grain radius, r_{nm} (nm), heliocentric distance, R (AU) and nuclear distance, r_n (km):

$$F_{nd} = 9.76 \times 10^6 r_{nm}^{-0.754} R^{-2.69} \left(\frac{r_n}{10}\right)^{-1.854} \quad (1)$$

The equation and figure both assume an ideal collection efficiency. Figure 2 shows that the collection of one grain of 1 μm radius on an area of 10 $\times$ 10 μm (or 100 grains on 100 $\times$ 100 μm) requires, on average, a 50-hour exposure under the assumed conditions. These quoted areas are the medium and the maximum scan areas, respectively, of the instrument. The medium scan area gives a resolution of 40 nm per pixel, which is reasonable for a topographic analysis. Searching a large area at low resolution can produce a dramatic reduction in exposure time by locating dust particles for later high-resolution imaging. For this reason, MIDAS includes a zoom-in capability. The zoom-in capability is based on on-board image processing and feature detection algorithms applied to an overview image, which result in a prioritised list of particles, their main geometric features and coordinates. Subsequent images will be made according to the coordinates identified by this process.

Let us compare the exposure times derived under the above mentioned conditions to the results on dust flux obtained by Weiler *et al.* (2004) for 67P/Churyumov-Gerasimenko. Our calculations for a 1 μm radius grain correspond to an area coverage of 3% and an area flux of 1.6×10^{-7} s^{-1}. Weiler *et al.* calculate a cumulative area flux of $\sim 3 \times 10^{-6}$ s^{-1} for all particles at 10 km nuclocentric distance during maximum activity, and state that the size range of a few micrometers contributes most to the area flux. However, the contribution of 1 μm size particles amounts to only $\sim$10% of the cumulative flux, so that their model results fall into the same order of magnitude as the earlier predictions for P/Wirtanen. The dust flux is also significantly reduced at larger heliocentric distances. There is still a large number of open questions on the size distribution, the evolution of dust production rate, and on he finally chosen Rosetta orbits around the comet, which all of them strongly influence the dust flux to the instrument and the exposure times. The estimates available so far can only help to design the initial exposure strategies, which will have to be refined during the mission.

4. Principle of an Atomic Force Microscope

An Atomic Force Microscope forms the heart of MIDAS. A wide range of 'scanning probe microscopes' has been developed since the advent of the Scanning Tunnelling Microscope (STM) in 1982. They all make use of a sharp tip scanning the surface of a sample and derive information from the tip-sample interaction. The interaction depends on the nature of the tip and is based on the electron tunnelling effect (STM)

or mechanical force (AFM). Combinations with electrostatic, magnetic or optical sensors in the near-field have also been developed. Using piezoelectric motion systems, the surface features can be resolved with atomic resolution yielding the topography and some additional material properties of the sample. In order to record topologies and investigate the material properties of cometary dust particles with nm resolution, MIDAS adopts non-contact, dynamic AFM as the main working mode.

The mechanical force of the tip-sample interaction results in a deflection of a cantilever to which the tip is attached. The sensitive measurement of this deflection is essential for the quality of the images. MIDAS employs piezo-resistive cantilevers that can detect their own deflection electrically and, thus, eliminate the need for additional sensing elements.

Figure 3 schematically shows the basic elements of an AFM: a piezoelectric scanner for cantilever movement, a tip mounted near the edge of the cantilever, a detection system for cantilever deflection, a feedback system to control the vertical tip position and a computer to control the scanner and acquire and process the data. In addition, a coarse approach system is needed to bring the tip to within the working distance of the piezoelectric scanner. The tip-sample interaction results from a combination of the short-range, repulsive atomic forces and the long-range Van der Waals force. The contact between the tip and the sample occurs when the overall interaction force becomes repulsive. At a tip-sample distance of a few Ångstrøm, which corresponds to the length of a chemical bond, both attractive and repulsive components cancel out and the interaction force becomes zero. Not only

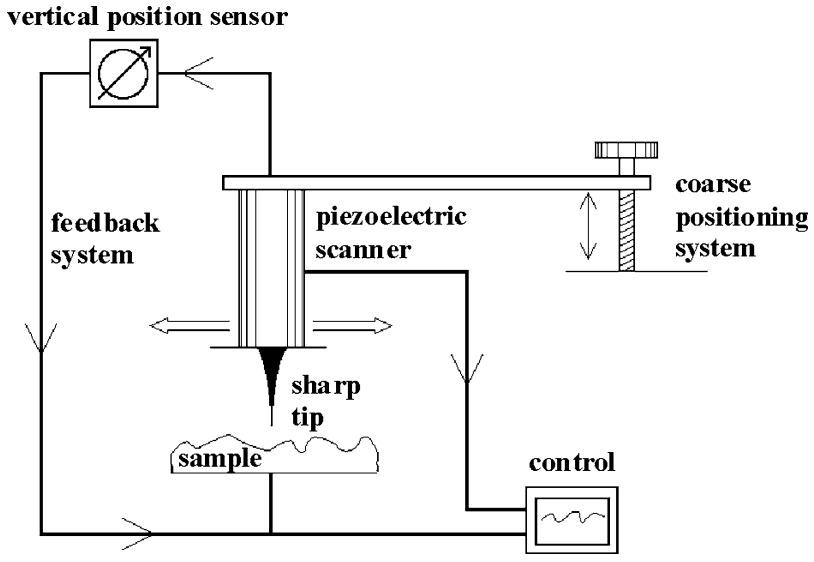

Figure 3. The basic elements of an Atomic Force Microscope.

mechanical forces may act on the tip, depending on its design. Magnetised tips, as partially implemented in MIDAS, will also be sensitive to magnetic forces.

4.1. AFM Operating Modes

Contact mode: the working point is set close to the repulsive force regime where the tip actually touches the surface. Typically, a force of the order 10^{-7}–10^{-6} N is exerted on the sample. Owing to the strongly increasing repulsive force at decreasing distances, the tip cannot penetrate deeply into the surface and the soft cantilever bends. However, the pressure exerted by the tip is high and soft samples, particularly, can be scratched or damaged.

Dynamic mode: the cantilever is excited at its natural mechanical resonance frequency ($\sim$100 kHz) at close distance to the sample. The amplitude of the cantilever vibration is of the order 100 nm. Depending on the operational setting, the tip may or may not touch the sample during each oscillation. At small tip-sample separation of the order 5–10 nm, the interaction of the electron orbits results in a weak attractive force, and the resonance frequency of the cantilever changes owing to a virtual increase of its spring constant. The quantity thereby measured is not the force directly, but its gradient. As in the contact mode, vertical resolution in the nm range can be achieved. The force applied by the tip to the sample is of the order 10^{-8} N. This relatively small force and the absence of lateral forces makes damage to the tip less likely, and the lifetime of the tip increases considerably. The lateral resolution obtained in dynamic mode is comparable to that of the contact mode. However, dynamic mode images often represent not only the topography, but also to some extent the elastic properties of the sample under investigation. The mechanical resonance frequency of the cantilever has to be determined before any measurement in dynamic mode.

Magnetic force microscopy: This derivative of atomic force microscopy (Martin and Wickramasinghe, 1987) records a magnetostatic force between sample and a magnetised tip. Four of the MIDAS tips have been coated with a thin layer of cobalt. The deflections of their cantilevers then result from a combination of mechanical and magnetic forces, which can be separated by measurements at two different tip-sample distances. These tips map the magnetic structures of the particles in addition to the topographies.

5. Hardware Description

5.1. Overview

Riedler *et al.* (1998) documented the status of the investigation shortly after the selection for the Rosetta payload. At that time the key elements of the instrument had

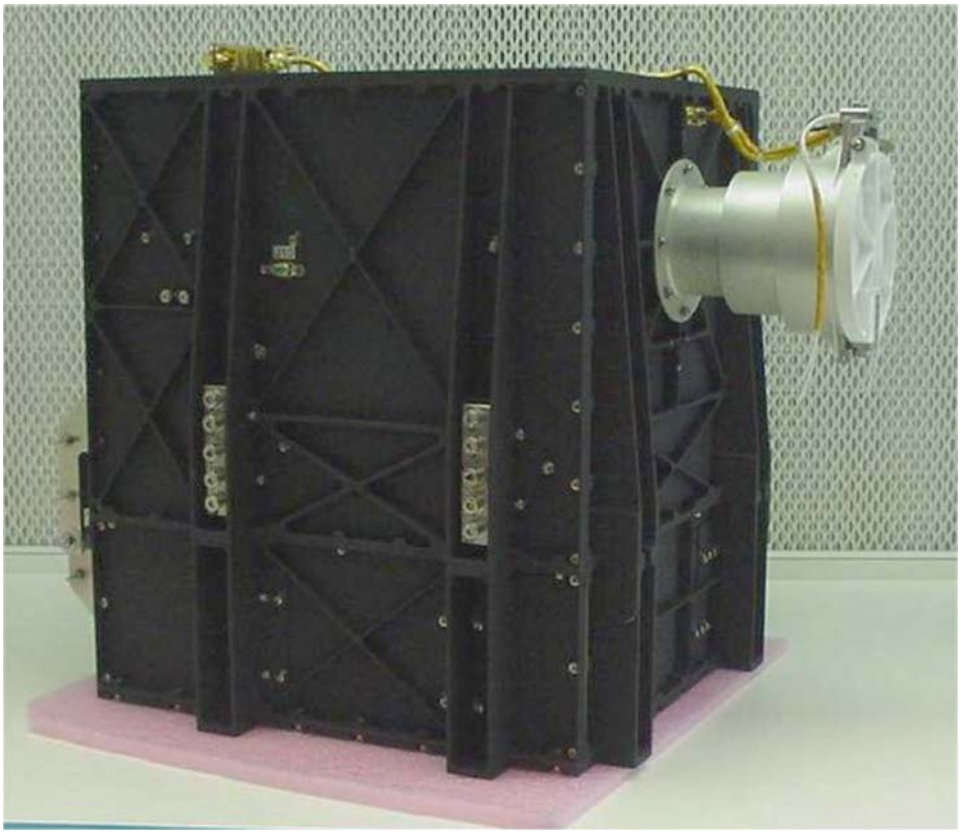

Figure 4. The instrument with the funnel cover closed in launch configuration.

been defined, but the detailed design had only been started. The MIDAS instrument in its flight configuration consists of a single mechanical unit (Figure 4). The top part of the main box houses the elements of the AFM and the system to collect and transport the dust samples from the exposure position to the head of the microscope (Figure 5). The structure is made out of ribbed aluminium plates. A funnel-shaped dust intake system, which protrudes through the outer spacecraft wall, is attached to the upper part of the box. An external cover protects the internal elements against contamination during ground operations and launch. A shutter at the outer end of the funnel controls the exposure time of one facet at a time on the dust collector wheel inside the box. This wheel can be rotated and translated to transport the dust samples to one of 16 sensor elements (cantilevers) in the AFM after exposure. The array of cantilevers is fixed to the Z microscope stage, which is attached to the high-resolution XY positioning stage. All stages are driven by piezoelectric systems, and the displacements can be measured by a strain gauge and capacitive sensors. In addition, the voltages applied to the piezoelectric actuators provide the

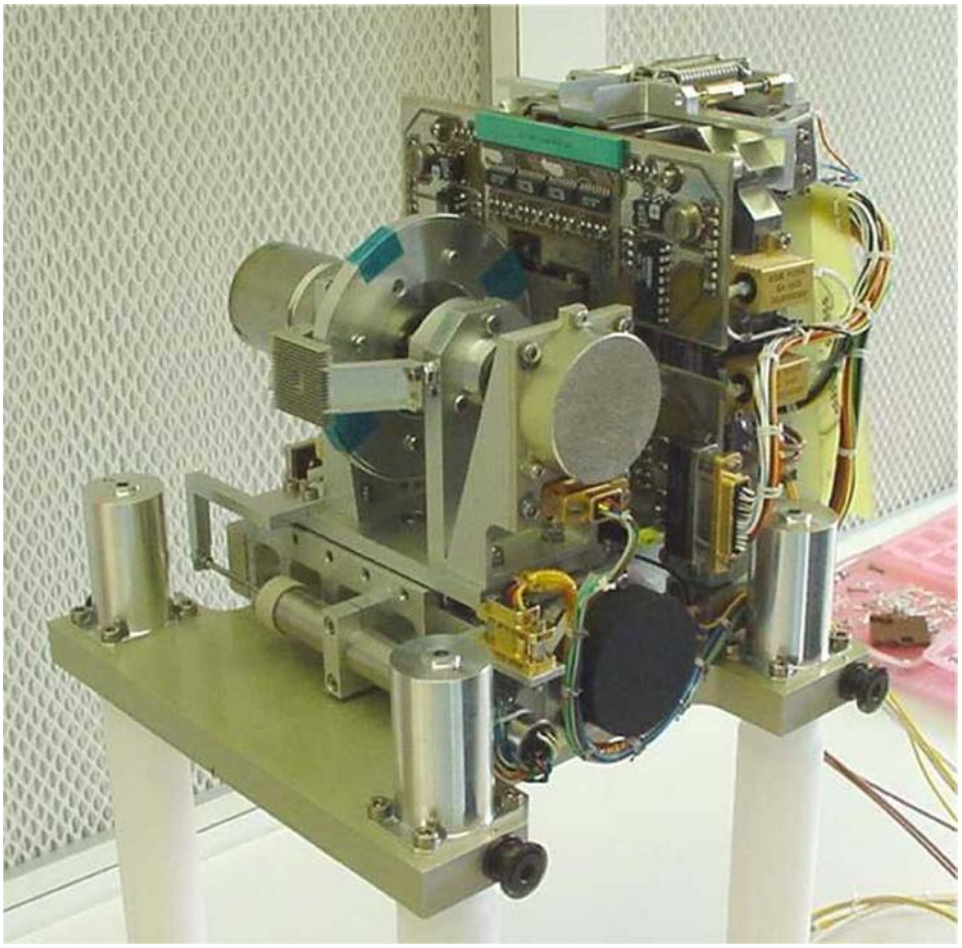

Figure 5. The internal dust collecting and microscopic unit.

same displacement information through the respective calibration curves. To begin the imaging process, the XYZ-stage is brought into contact with the sample on the dust collector wheel by the approach mechanism. As soon as the selected cantilever senses contact with the sample (indicated by a deflection of the cantilever in contact mode, or a change of amplitude in dynamic mode), the scanning operation can start. After the measurement, the XYZ-stage has to be retracted, and another approach procedure has to be performed before the measurement on another area. The 16 available needles have slightly different characteristics and shapes, and four out of them are additionally sensitive to magnetic forces. The degradation of a needle during scanning and the available lifetime very much depend on the operating parameters and the sample. The selection of a particular needle is achieved by moving the linear stage to position the dust collector wheel in front of the respective cantilever.

As the measurements by the AFM are sensitive to microvibrations induced by other active mechanisms aboard Rosetta, the AFM element is fixed to the base plate of the box by four studs of highly flexible silicone material with a high damping capability. During ground operations and launch, the AFM platform was locked in its zero position by a clamping device, which is unlatched after launch by a mechanism using paraffin actuators.

The lower part of the instrument serves as the electronics box, which could be decoupled from the upper section to help the assembly process. Most of the printed circuit boards are located in the lower section, but a few sensitive amplifiers reside in the AFM area close to the sensors. The electronics box has a connector panel for redundant electrical interfaces to data, power and checkout. Some additional connectors, e.g. for pyrotechnic actuators, are mounted on the AFM box. The electronics box has eight lugs for mounting on the spacecraft payload platform.

The realisation of this instrument was the responsibility of an international consortium lead by the Space Research Institute of the Austrian Academy of Sciences, which is also in charge of the electronics hardware and software, the electrical ground support equipment, flight operations and data processing. Austrian Aerospace was the major contractor for the flight electronics. The ESA/ESTEC Space Science Department was responsible for the development, production and testing of all mechanisms, the instrument box and, in particular, the AFM, with the exception of the cantilever module and the target wheel with the dust collection surfaces. These latter components were developed by the ARC Seibersdorf research GmbH (Austria). The cantilevers were designed and produced at the University of Kassel.

5.2. Dust Intake System

5.2.1. *Cover and Funnel*

The dust intake system consists of an external cover protecting a funnel. The cover's main purpose is to protect the funnel and the shutter's outer surface from contamination during final launch preparations, when cooling air was blown directly onto the instrument for several days. However, the cover is not hermetically sealed. After launch, it was opened by a pyrotechnic actuator.

The funnel, firmly attached to the side wall of the instrument box, provides a defined aperture through the spacecraft wall (Figure 6). Its inner structure and surfaces inhibit secondary reflection of incoming dust particles. The inner edge points towards the entrance of the shutter, which operates to control the exposure time for the selected facet on the dust collector wheel.

5.2.2. *Shutter*

The shutter is a movable system to control the exposure of the collector to the ambient dust flux. It also preserves the internal cleanliness of the microscope during all phases following the integration of the microscope. It is based on a piezoelectric mo-

tor rotating a cylinder with two opposing openings. A microswitch senses whether the dust inlet opening is open or closed. The same type of piezoelectric motor rotates the dust collector wheel.

5.3. Robotics System

5.3.1. *Overview*

The robotics system ensures that dust particles are collected on a predetermined surface area and transported in a controlled manner to the AFM's scanner head. Its

(a)

Figure 6. Location of MIDAS, seen here on the Rosetta Structural Thermal Model at ESTEC.

(*Continued on next page*)

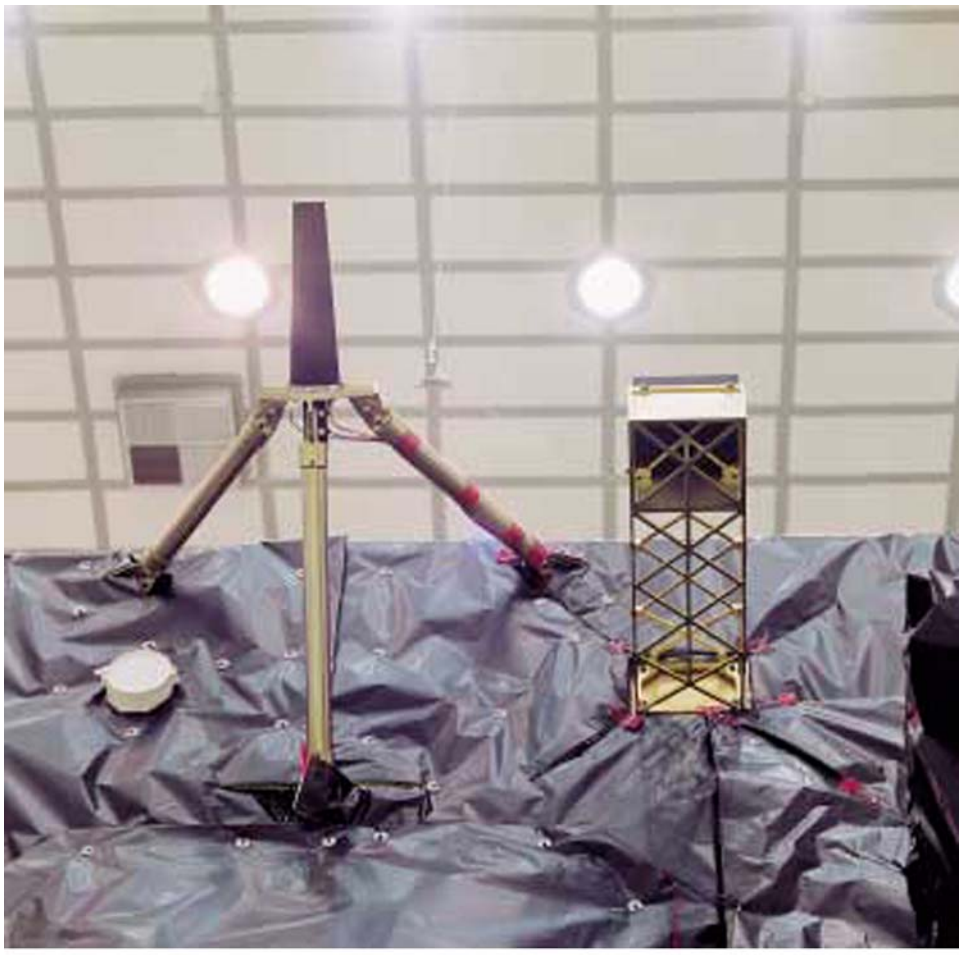

(b)

Figure 6. (*Continued*).

elements are on a rigid base plate that connects with the outer housing through a mechanical damping system. Three motions are required:

- a rotation to bring the exposed area of the dust collector wheel in front of the scanner head,
- a linear translation of the collector wheel of up to 30 mm in axial direction to one of the tips of the scanner head and for coarse positioning of the scanning area within the exposed facet,
- a translation of the scanner system of about 1 mm, perpendicular to the previous translation, to move the tip to the scanning area on the dust collector wheel.

5.3.2. *Dust Collector Wheel*

Dust particles are collected on one of the 64 facets on the circumference of the dust collector wheel, which has a diameter of 60 mm and a thickness of 1.4 mm (Figure 7). Each facet is sized 1.4 × 2.4 mm with an area of about 3.5 mm^2. A collimator defines the exposed area. For measurement, the area of interest has to be positioned under a tip of the scanner head. This is achieved by rotating the collector wheel by a piezoelectric motor. An attached incremental shaft encoder with a resolution of 1024 positions per rotation and a reference position allows an accurate determination of the wheel's position. A radial loaded shaft (a preloaded backlash-free ball bearing) eliminates clearance in the rotation system. Three of the 64 facets carry calibration gratings that can be used to check the condition of the tips on the scanner head and to calibrate the displacement of the scanner head.

5.3.3. *Surface Material for the Dust Collector Wheel*

The collection of dust from the comet must be done very efficiently in order to minimise the exposure times. High efficiency also permits more distant orbits around the comet, thereby reducing the contamination of spacecraft surfaces. The requirements for the wheel surfaces are:

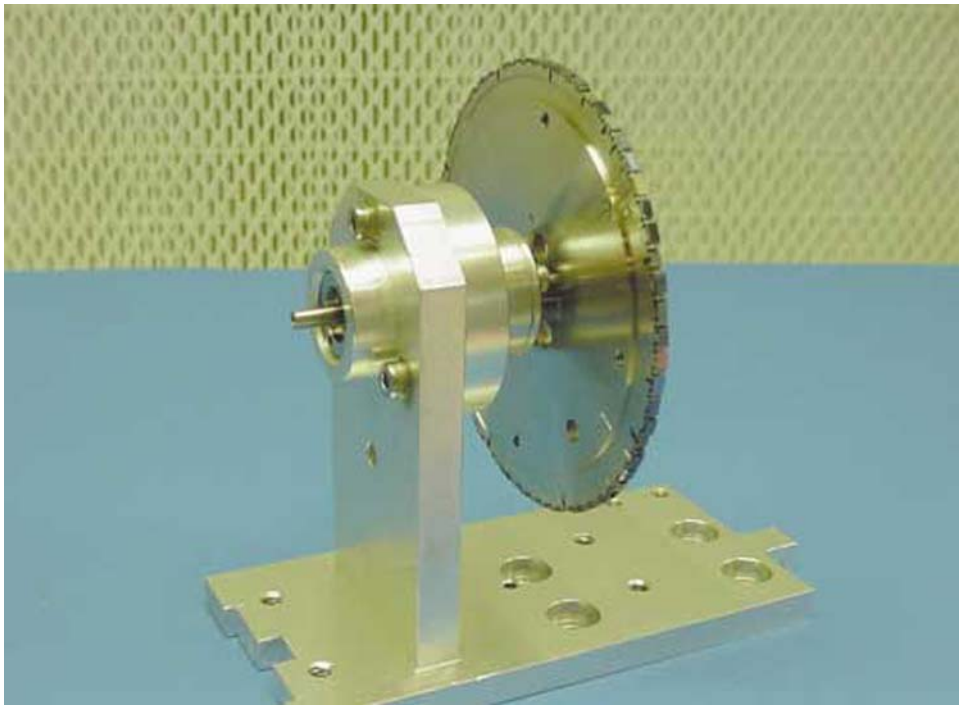

Figure 7. The dust collector wheel, with 64 mounted facets. The wheel is 60 mm in diameter.

TABLE I

Measured roughness of the collection facet surface coating.

Property	Size (nm)
Maximum peak/valley distance	5.4
Root mean square roughness	0.4
Average deviation	0.3
Median height	1.7
Average height	1.6

- good adhesion on substrate material,
- good catching efficiency for high speed (up to several 100 m s^{-1}) dust grains,
- high surface smoothness to avoid artefacts in the AFM,
- stability under vacuum and temperature excursions.

After experimenting with topographically nano-structured surfaces and various coating materials, the optimum collection surface material turned out to be a 'sol-gel' coating on highly polished pure silicon chips. This coating consists of a flexible silsesquioxane-based resin, prepared via the fast solgel routine from methyltrimetoxysilane and tetra-methoxysilane. This resin has also been suggested for atomic oxygen-protective coating materials. The solgel was spin-coated on to 300 μm-thick silicon chips at 1000 rpm. The layer thickness under these conditions was measured to be 14 μm. These coatings have been proved to have high collection efficiency (see below) and low surface roughness, which was determined using an AFM (Table I). The coated chips are bonded to 61 facets on the sampling wheel. Three of the facets carry calibration samples for the AFM, allowing to calibrate X/Y deflection and height length scales and to estimate the AFM tip radius.

5.3.4. *Linear Translation Stage*

The dust collector wheel with motor and encoder is located on the mounting plate of the positioner. The longitudinal movement is performed by a linear stage driven by a travelling wave piezoelectric motor through a preloaded backlash-free ball bearing spindle with a pitch of 1 mm. Guidance is provided by a crossed roller bearing. The position of the linear stage is measured with a Linear Variable Differential Transformer (LVDT). The need for a translational movement of 30 mm ensues from the need to select one of an array of 16 tips with 1.6 mm intertip distances, and for coarse positioning of the scanner with respect to the facet under investigation. In the latter case, the translation remains within the thickness of the collector wheel ($<$1.4 mm). The linear translation stage also has a launch lock position and two integrated microswitches to protect against over-ranging.

5.3.5. *Approach Mechanism*

After a rotation of the dust collector wheel, the scanner has to perform a carefully controlled approach (in steps of $\sim 1\ \mu$m) to the surface until contact is made between the surface and the tip. The scanner head is fixed on one side of the sample approach system. The approach is achieved by widening a wedge system with a shaft with bearings. The linear translation of this shaft is achieved by a fine threaded shaft coupled to a DC motor with a gearbox. This motor-gearbox-threaded shaft system is contained in a pressurised (1 bar) and hermetically sealed container. The expansion is enabled by a very flexible bellow. The translation is limited by an upper and lower microswitch. A translation of 5 mm gives an approach at the centre of the XYZ-stage of 1 mm. The displacement is measured by an LVDT. The system is designed for high reliability. The approach mechanism has to be activated before and after each scan in order to avoid any damage to the tip. The approach mechanism has a launch lock position.

5.4. CANTILEVERS

For investigating dust particles with heights smaller than $\sim 7\ \mu$m, an AFM instrument can characterise the topography with high lateral field resolution. The design has to take the following important aspects into account:

- the spring constant and the geometry of the cantilever (length, height, and width) should match the expected mechanical properties (E-modulus) of the dust particles,
- the tip geometry (aspect ratio and tip shape) shall take into account both the expected topography of the particles and the lifetime of the tip,
- for dynamical modes the resonance frequency shall provide good sensitivity, but also comply with the bandwidth of the electronic amplifiers.

The cantilevers employed for MIDAS are fabricated from double-sided polished silicon wafers in a multi-step process using dry and wet etching methods, which produce cantilever structures including the needle with well-defined properties. Figure 8 shows an array of four cantilevers.

In a conventional AFM, the motion of the cantilever with the tip is measured using optical detection schemes (e.g. interferometry, triangulation). These techniques require a manual adjustment with respect to the optical detection beam. To avoid this adjustment procedure, MIDAS utilises a novel detection method whereby the cantilever is associated with an electrical sensor which converts the mechanical displacement of the tip into an electrical signal. For this, four piezo-resistors are included at the connection area between the cantilever and the bulk silicon, the location with maximum stress. These resistors form a classical Wheatstone bridge. A passivating film protects the resistors against environmental condition. Four aluminium pads at the rear end of the bulk silicon provide the electrical connection. A

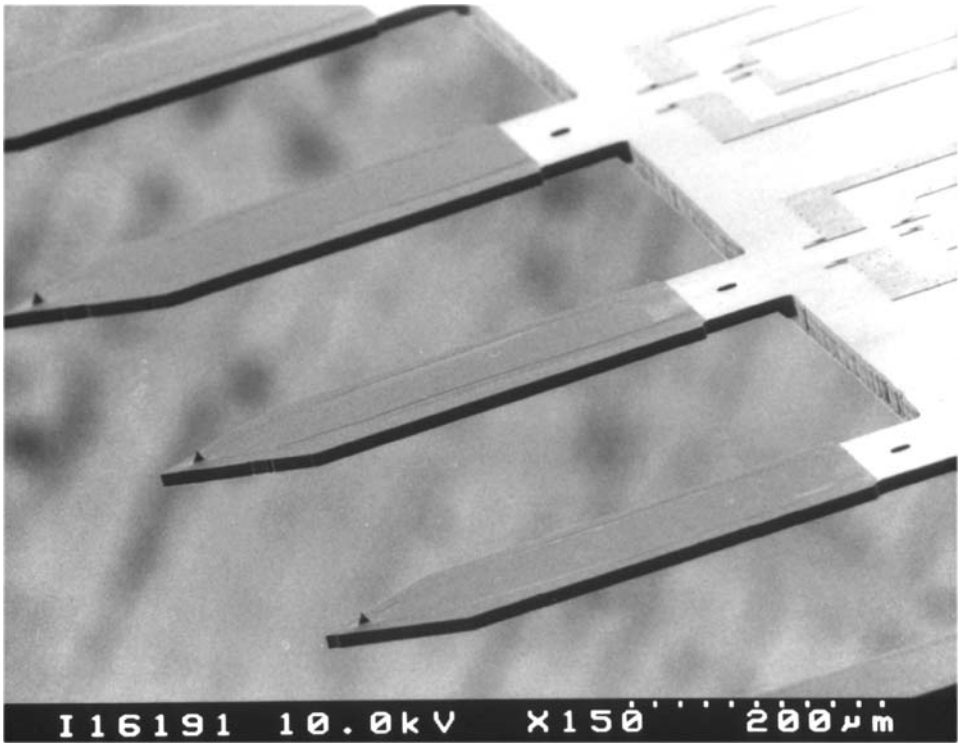

Figure 8. Array of 4 cantilevers.

single cantilever is a bar of 600 μm length and 150 μm width, with a triangular shape at the end and a thickness of 15–20 μm. The resonance frequency is $\sim$100 kHz. When the cantilever vibrates, the mechanical stress at its base is converted into an electrical output voltage via the piezo-resistive effect of the silicon material. This voltage is a direct measure of the tip motion. The sensors are suitable for both contact and dynamic modes.

5.5. SCANNER SYSTEM

5.5.1. *Scanner Head*

It is recognised that the tips are the most critical item in terms of lifetime. Although they have long lifetimes as far as their scanning time is concerned, it must be recognised that mechanical failures and absolute scan lifetime are limiting factors. MIDAS is therefore equipped with 16 tips to provide sufficient redundancy over Rosetta's mission time. All 16 cantilevers, organised into four chips of four cantilevers each, are mounted on a carrier board sitting on the top of the Z piezo stack. An additional, small, piezo that provides the excitation near the resonance frequency of the cantilevers, is mounted close to the cantilever arrays.

The carrier board consists of two parts: the carrier board made from ceramics as a support structure for the individual cantilever chips, and a small printed circuit board for the electrical interconnection. To avoid thermally generated mechanical stress, the ceramic structure provides physical properties close to that of the silicon of the cantilever arrays. In addition, the ceramic substrate provides the electrical connection from the cantilevers to the printed circuit board by use of thick-film technology. The connection from the cantilever to the ceramic substrate uses bond wires.

5.5.2. *Scanner Table*

The scanner system is attached by an intermediate plate to the sample approach mechanism. The scanner system contains a 3-axis piezoelectric scanner. The maximum scanning range is 100 μm in the X- and Y-axes, but typical scan sizes are much smaller ($2 \times 2\,\mu$m to $20 \times 20\,\mu$m). The maximum extension in the Z-axis is $\sim$10 μm. The lateral resolution in closed-loop using the feedback signal from the capacitive displacement sensors is 3 nm. The Z-axis position is measured by a strain gauge, and features of 0.1 nm height can be resolved. The scanner head with the array of 16 tips is mounted on top of the scanner. The lateral distance between the tips (1.6 mm) is slightly larger than the thickness of the dust collector wheel (1.4 mm) to ensure that only a single tip can make contact with a sample at any time.

The maximum height of a particle that can be fully characterised depends on the shape and dimensions of the tip. The presence of too large particles may cause image artefacts, i.e. the cantilever instead of the tip can touch the particle and disturb the image. The current tip/cantilever design puts this limit at $\sim$10 μm. Current dust models predict that the abundance of large particles decreases with particle radius – so large particles are rare. Using exposure times tailored to small particles means that the probability of a large particle within the scan field is low, and interference with the cantilevers is unlikely.

5.5.3. *Clamping Mechanism of the Scanner Stage for Launch*

During launch, the XYZ piezoelectric scanning stage was locked by a clamping mechanism on each side of the stage. These clamps secure the inner part of the XYZ stage that moves during image acquisition. A pre-loaded steel braid locks the clamps. The redundant actuators (two per clamp) cut the wires. A spring on each side of the clamp forces the levers to move backwards and remain in a fixed position.

5.6. Mechanical Damping System and Clamping Mechanism of the AFM Base Plate

5.6.1. *Mechanical Damping System of the AFM*

The high resolution of MIDAS requires a mechanically stable design and environment. Vibrations are generated by satellite manoeuvres or mechanisms such as

reaction wheels, gyroscopes, tape recorders, antenna motors and solar arrays. However, susceptibility to microvibrations applies only to the scanning operations and not to the interleaving exposure periods. Intermittent vibration can be tolerated if a suitable timing scheme is followed. According to the current analysis of Rosetta's microvibration sources, the propagation of vibrations to MIDAS and their effect on its measurements, the dominant source of mechanical noise will be the movements of the high gain antenna and reaction wheels. Accelerations caused by these sources of the order of 10^{-3} g are predicted at the mechanical interface to MIDAS. The scanner system of MIDAS has been trimmed to high stiffness to reduce the sensitivity to microvibrations.

Accelerations of the predicted magnitude would still permit a resolution of 1 nm. In order to provide some safety margin, provisions for mechanically decoupling the AFM from the box have been made in order to further reduce the effect of microvibrations. The dust collector wheel and the scanner system are mounted inside the AFM box on a mechanically decoupled base plate, held in position by four silicone rubber elements with high damping capability. Noise at frequencies higher than the internal resonance frequency of the damping system ($\sim$5 Hz) is effectively damped.

5.6.2. *Clamping Mechanism of the AFM Base Plate for Launch*

During ground operations and launch, the AFM platform was locked in its zero position by four spring-loaded clamps. Zero position means that the silicone dampers are not loaded. After launch, the clamps have been released in two pairs by one paraffin actuator each. The connecting cable between two clamps forces the movable levers of both clamps to release the mechanism at the same moment.

The clamp itself consists of an upper and a lower section. The two studs, connected to the base and cover, respectively, are held between the clamps. The movable lever is attached to the lower clamp. Four disc springs push four pins against one stud. One leaf spring connecting the upper and lower clamp forces the mechanism to open and release the damping mechanism.

5.7. ELECTRONICS

The MIDAS electronics are distributed over six printed circuit boards. The electronics box contains four boards with the power converters, the processor, and analogue signal conditioning circuits. A board holding the capacitive sensors for the scanner table and several motor drivers is mounted beneath the base plate of the AFM box. The sixth board with the pre-amplifiers for the sensors is mounted at the scanner table.

Figure 9 shows the functional blocks of the electronics, sensors and actuators. The microprocessor (MP), an HS-RTX2010 real-time express microcontroller, controls the scanning process and all mechanisms, collects the scientific and housekeeping data, and handles the command and data interfaces to the spacecraft. For mass

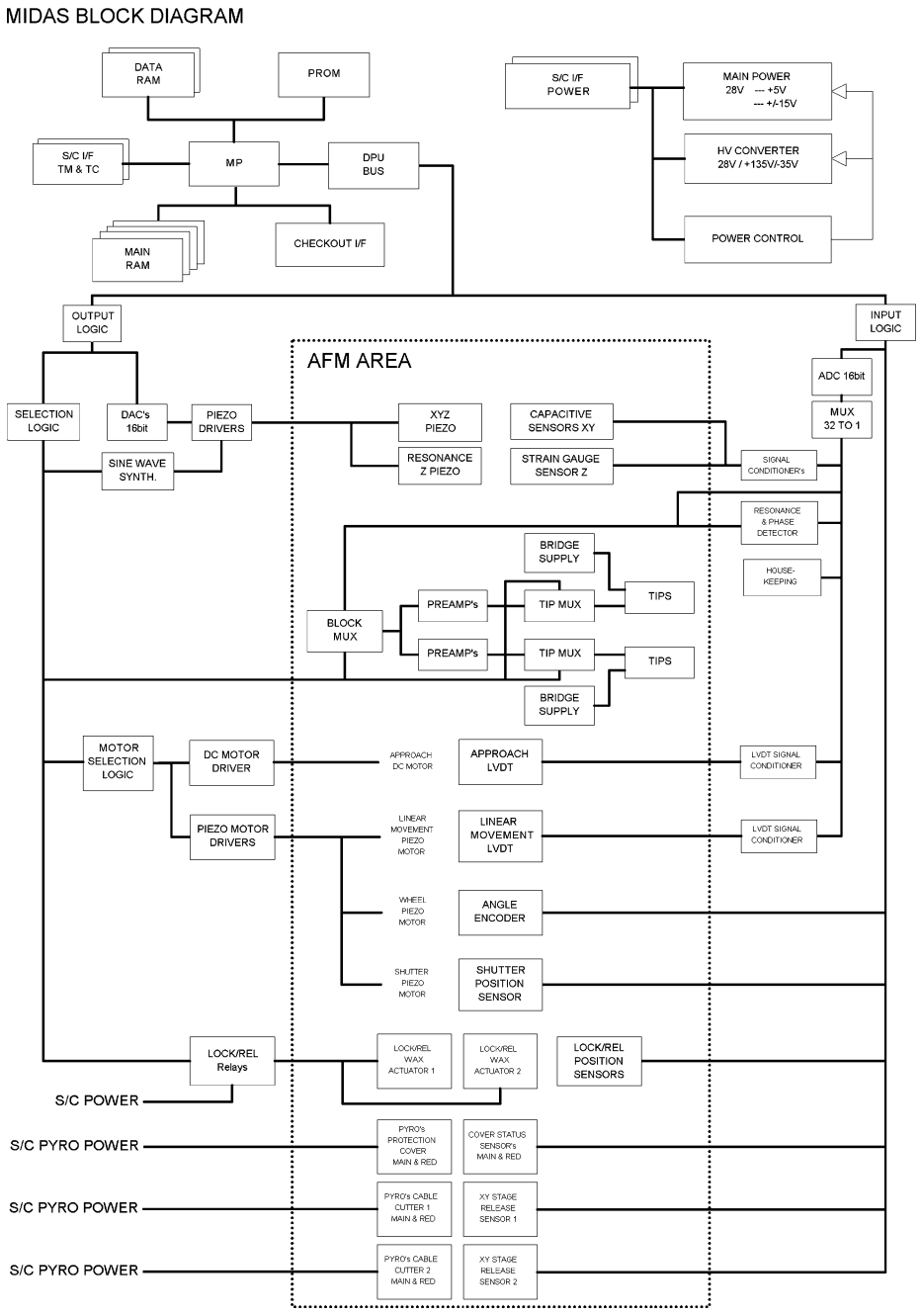

Figure 9. MIDAS functional block diagram. ADC: analogue-to-digital converter, DAC: digital-to-analogue converter, DPU: digital processing unit, HV: high voltage, I/F: interface, LVDT: linear variable differential transformer, MP: microprocessor, MUX: multiplexer, RED: redundant, S/C: spacecraft, TC: telecommand, TM: telemetry, WAX: paraffin wax actuator.

reasons, redundancy in the electronics is limited to the spacecraft interfaces and the memory. Reliability is ensured by the use of appropriate electronics components in all critical areas. The dotted area in the centre of Figure 9 marks units located in the upper part (AFM) of the instrument box. Apart from the scanner and pre-amplifiers for the cantilevers, several motors and actuators have to be controlled.

The most demanding requirements have been set for the capacitive sensor electronics. The motions of the scanner system must be controlled to a resolution of a few nm over a range of 100 μm. The position is measured by a capacitive sensor in each direction. As the capacity varies as little as between $\sim$3 pF and $\sim$10 pF, the electronics have to measure and control the capacities to a resolution of 10^{-16} F. Not only resolution, but drifts owing to thermal effects and ageing also have to be kept low, and recalibration during flight is planned. Another uncommon functionality is required for the driver electronics of the piezoelectric motors. These motors operate by friction between the electrically-stimulated piezoelectric stator and rotor. For high efficiency, the frequency of excitation (several tens of kHz) has to follow the mechanical resonance frequency and its variation with temperature.

The digital processing unit (DPU) has to perform several tasks in parallel, the most time-critical being the response to interrupts triggered by the interfaces to the spacecraft and the operation of the scanner. The latter would be controlled by its own processor in a laboratory AFM. For MIDAS, high priority has been given to ensuring a long lifetime of the AFM tips. For this reason, the Z-position (height) of a tip has to be controlled very carefully while scanning over the sample, avoiding large deflections of the cantilever and correspondingly high forces on the tip. The control loop in MIDAS is fully digital. The DPU's other main task – processing the data – is largely performed between individual scans, but limited time is also available during a scan, when there are waiting times owing to relaxation of the piezos. A total of 1.5 MB of RAM is available for code and data, out of which 1 MB can be allocated to stored image data before they are transmitted.

5.8. Electrical Power Management

Owing to Rosetta's limited power resources and the high power consumption of several MIDAS mechanisms, a power-switching scheme has to be implemented. A basic power level of 8.3 W in standby mode is required by the DPU for general control purposes, data management and housekeeping. The three piezoelectric motors were selected because of their low mass and power requirement. Nevertheless, if these motors are operated in continuous mode they consume more than 10 W. However, as MIDAS does not require their full moment, they are operated in bursts of $<$1 ms. The average power is thus reduced to 1–3 W, depending on the duty cycle.

The power-hungry functions during scanning arise partly from the piezoelectric scanner table itself, but mainly from the Wheatstone bridge of the active cantilever,

the preamplifiers, and the position sensors (capacitive sensor electronics and a strain gauge). The power to these components can be switched off after scanning, releasing some power for the positioning of the dust collector wheel. The power consumed during scanning amounts to ∼13.4 W.

In addition to the regular operating modes, there is the release of the launch lock for the AFM base plate. This mechanism is driven by a pair of paraffin actuators that must be heated for a few minutes, and consumes ∼10 W. As the DPU and some other driver circuits have to be active simultaneously to control and monitor the operations, the total power consumption during this release operation is ∼19 W.

6. Operating Modes and Onboard Software

In order to fulfil its scientific objectives, MIDAS has to acquire and analyse samples of cometary dust at regular intervals throughout all phases of the mission, in particular the nominal payload operation phase and the extended mission phase. At first, the selected facet of the dust collector wheel has to be exposed to the ambient dust flux until the required surface coverage by dust is achieved. The best coverage value remains to be determined experimentally and will also depend on the type of analysis planned (imaging of individual particles or statistics). Current estimates indicate a surface coverage of 0.1% should be sufficient for most purposes. The required exposure times range from fractions of an hour during high cometary activity at close distances to the nucleus (few cometary radii) to several days during moderate activity and/or larger distances. Longer periods should be avoided in order to ensure proper coverage of the comet's evolution. Exposure should also be scheduled simultaneously with measurements by other dust instruments. Apart from the facet selection and shutter operations at the beginning and end, MIDAS may be left unpowered. Alternatively, if it remains in standby mode, it is able to listen to broadcast messages that may be used to adjust the exposure time autonomously. If MIDAS is powered during exposure, it may also simultaneously process previously obtained images. After exposure, the shutter is closed and the target wheel can be turned to another position for the exposure of another facet, or a facet can be placed underneath the scanner head.

AFM images of the exposed target areas are obtained by scanning. At the beginning of the scan mode, an area on the collector wheel is selected by rotating the chosen facet under the scanner head. In each scan, only a small part of the exposed surface is imaged by the microscope. The selection of scan areas within a facet is achieved by fine control of the angle and lateral position of the wheel. A single exposure period will be followed by several scanning operations on the previously exposed facet at varying resolutions. It is also possible to scan or rescan facets that have been exposed much earlier. The time needed to scan a single area on a facet depends on the operational settings and is of the order of several hours.

Processing and transmitting the acquired data is typically performed after completion of a scan (image acquisition). Typically, processing time is short compared to the image acquisition time. The baseline MIDAS operations involve alternating between exposure, scanning and processing, but data collection simultaneously with the processing and transmission of collected images is also possible. Some images will be reduced to simple statistical parameters for transmission (for example, the number and sizes of dust grains), while others will be studied at full resolution.

The standard modes for exposure, scanning, and image processing as well as the associated positioning of the target surfaces are complemented by modes for checkout (e.g. occasionally to exercise the piezoelectric devices during Rosetta's cruise) and in-flight calibration.

The MIDAS software is structured into a low-level software kernel and a high-level main program. Every time the instrument is switched on, the kernel program is loaded into the Random Access Memory (RAM) and executed. After a successful check of the Electrically Erasable Programmable Read-Only Memory (EEPROM), the main program is started and the instrument enters standby mode. The software kernel handles the interface between the hardware and the main program, basic telecommand processing, generation of basic housekeeping telemetry, software maintenance and uploads, timing and low-level control of the hardware. Main program tasks include high-level instrument control, scientific and extended housekeeping data generation, and image processing.

Control of the instrument relies on sequences of low-level commands combined into larger packets. Recognised packets are processed with high or normal priority, depending on the telecommand type. Commands with high priority are executed immediately. They include time-critical commands, such as program abort, error reporting, and all commands processed by the kernel such as telecommand acknowledgements. Commands with normal priority are stored in a command buffer and executed sequentially. The low priority buffer is used for housekeeping and science data transfer where the packets are grouped into larger blocks. Two different subtypes of housekeeping data packets and six subtypes of science data packets have been defined. Science data packets are generated during or after acquisition of an image and processing of the image data. In general, data from one image will extend over many packets, depending on the resolution.

Among the routinely used modes, only the scan mode produces raw science data that are stored temporarily in instrument memory. The size of an image can be set to multiples of 32 pixels in each direction, with a maximum of 512 pixels. A typical single image of 256×256 pixels requires 128 Kbyte of memory. As 1 Mbyte is available for raw data, eight typical images can be held. Onboard image data processing is foreseen for two main reasons:

- reduction of the data volume to comply with the limit of 100 bit s^{-1} in mission phases with short exposure time and intensive scanning (i.e. data acquisition),

- identification and characterisation of dust grains to determine the coordinates of following scans (zoom-in).

Limited onboard processing power constrains the possible algorithms to background (i.e. target surface) determination and subtraction as well as characterisation of particles according to area, volume and elongation. The zoom-in capability enhances the performance of the instrument, but it relies on small thermal drift motions between subsequent scans.

7. Laboratory Studies

7.1. Dust Loading Experiments

Dust loading experiments and studies of dust collection efficiencies have been carried out during the development phase of the instrument. The dust accelerator used for these experiments at ARC Seibersdorf research GmbH is shown schematically in Figure 10. It consists of a 60 cm-long stainless steel acceleration tube with 2 mm inner diameter (ID). The accelerator tube can be interrupted by a sliding valve. The valve consists of a brass plate, sliding between a pair of O-rings, with a central diaphragm of diameter equal to the tube ID. The left section of the tube is usually at atmospheric pressure and the right section leads into a vacuum chamber, at the opposite end of which the samples are mounted on a linear manipulator.

Particles are loaded into the entrance funnel of the acceleration tube. The valve is manually pushed to its end position with a speed of about 1 m s^{-1}, thereby opening the passage through the accelerator tube for about 5 ms. Air streaming through the tube into the vacuum chamber accelerates the particles to speeds increasing with decreasing particle size. The dust beam exiting from the acceleration tube subtends a cone angle of about 90°. This beam is preliminarily collimated by a plate, extending almost across the full ID of the vacuum chamber, so that stray dust is prevented from entering the sample section of the vacuum chamber. The central section of the dust beam passes through the central diaphragm (3 mm diameter) of the pre-collimator.

The target geometry of the accelerator is shown in Figure 11. The dust beam from the pre-collimator then passes through collimator 1 of diameter 3 mm. Following that is the actual sample manipulator. The sample foils are mounted on the sample holder. The final collimator 2 plate is mounted 5 mm in front of the sample holder. The calibration foil is mounted on the upstream side of collimator 2, containing an array of five holes of 1 mm diameter separated by 5 mm. The relative position of collimator 2 and the sample holder is fixed. Independent samples may be mounted on the sample holder behind each of the collimator holes. The complete assembly is mounted on a linear vacuum feedthrough, allowing positioning of a selected hole in the final collimator under the dust beam. The dust beam passes the hole and

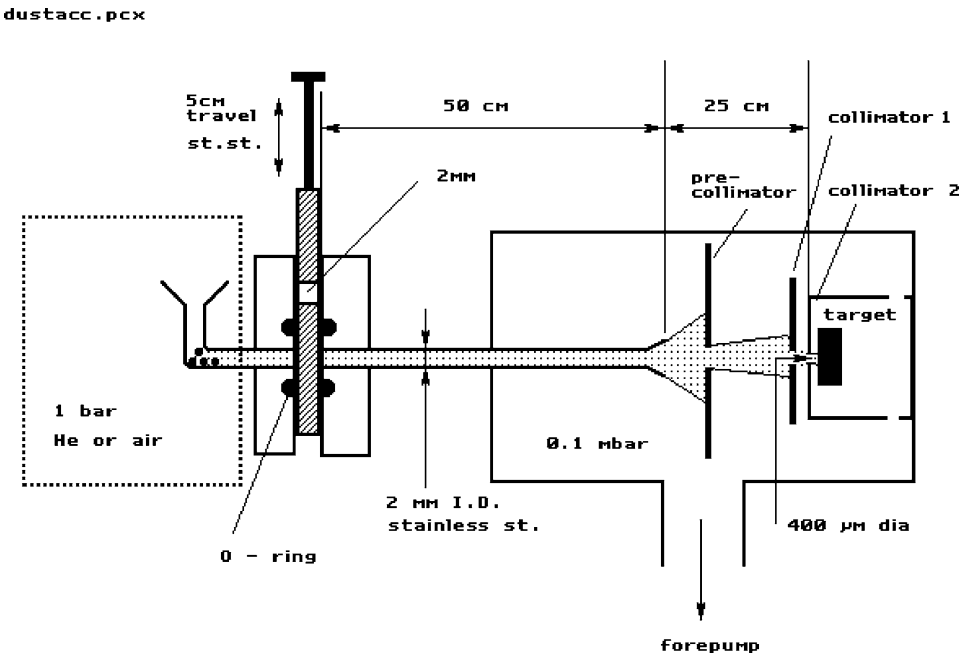

Figure 10. Schematic of the laboratory dust accelerator.

is (partially) deposited on the collection surface. Five independent dust exposures may be done before mounting new samples on the sample holder. The calibration foil collects particles with an efficiency approaching 100% (silicone grease, carbon tape). By comparing collected particle number densities on the sample foils and on the calibration foil, the collection efficiency of the sample foil is determined.

The length and diameter of the accelerator tube are the main parameters determining the gas flow velocity and the speed of the particles. For 25 μm copper particles, the impact speed has been determined to be 70 m s^{-1} on an accelerator of identical dimensions as shown in Figure 10 at Bundeswehrhochschule, Munich (Germany) using laser anemometry. Velocities of smaller particles are higher: using analytical models for gas dynamic acceleration of particles, terminal speeds of 180 m s^{-1} can be expected for <1 μm particles, thus providing good analogues for the cometary impact speeds.

7.2. Collection Efficiencies

Figure 12 shows an AFM image of aluminium nitride grains (used as cometary dust analogues) of average diameter 0.5 μm, shot at 180 m s^{-1} on to the solgel collector surface, using the ARC Seibersdorf research GmbH dust accelerator. It can be seen from the images that the substrate is smooth enough to allow identification

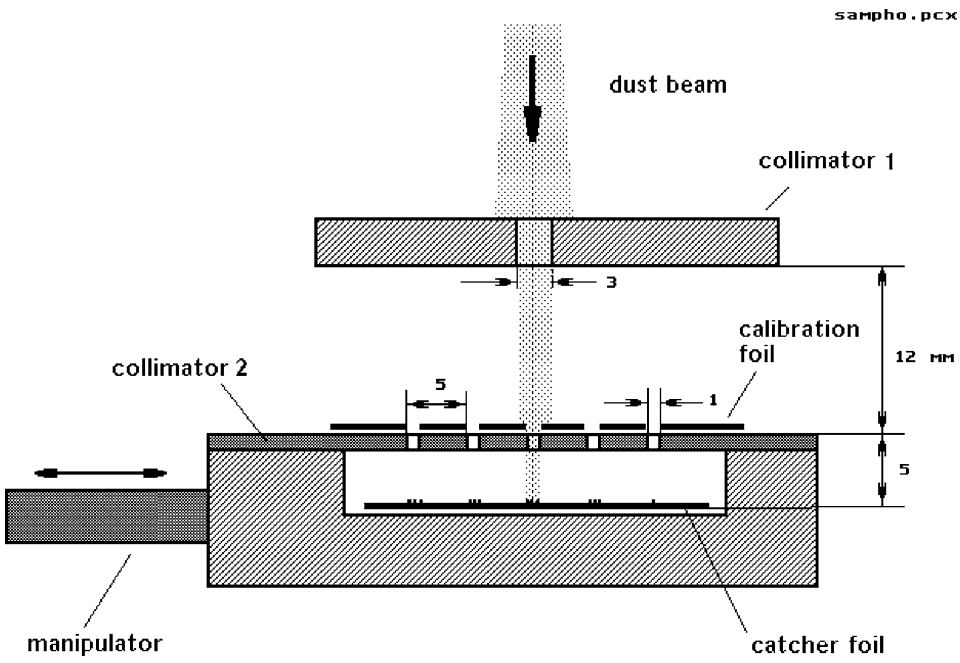

Figure 11. Target geometry of the ARC Seibersdorf research GmbH dust accelerator.

of $<0.01\,\mu$m grains, that the grains are sticking well enough to the substrate in order not to be removed during AFM imaging, and that single-grain AFM imaging (tapping mode) with high resolution is possible. The crystal planes of the captured particles are visible in Figure 13. On one plane, tiny subcrystals (see the insert in Figure 13) demonstrate the polycrystalline nature of the material. Even if particles are lost, they leave their imprints on the surface (Figure 13). The angular shape of the previously attached particles is still visible. In order to determine the collection efficiency, the number of particles deposited on equal areas of the collection surface and on a calibration foil were counted in the images of typical size $30 \times 20\,\mu$m. The collection efficiency is defined as the ratio of these counts, assuming that the calibration foil has a collection efficiency of 100%. The statistical evaluation of all the dust exposures on the solgel coating results in an average value for the collection efficiency of $\eta \sim 0.76 \pm 0.15$. The actual range of grain sizes in these tests reached approximately from $0.2\,\mu$m to $1.5\,\mu$m, sub-μm grains always are sticking together due to adhesive surface forces. In the accelerator however, wall collisions in the acceleration tube destroy most of the clusters so that single grains are the largest fraction of the adsorbed particles which can be observed on the substrate. Still, clusters of grains may be observed on the deposits, which astonishingly resemble "fluffy" IDPs.

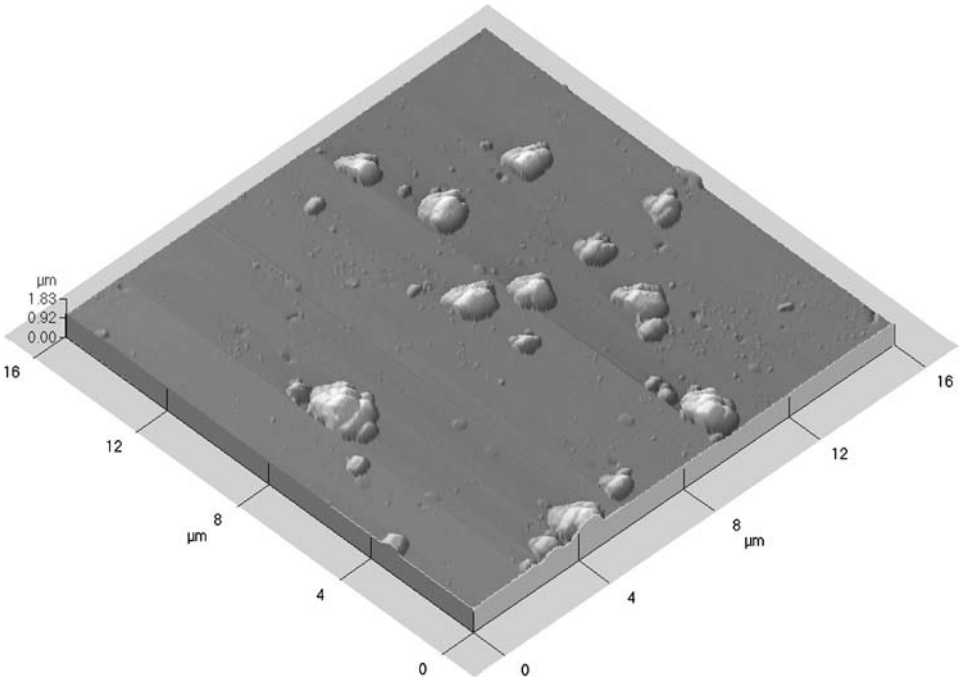

Figure 12. AFM image of Aluminium nitride (Al_2N_3) grains deposited at 250 m s^{-1} on 14 μm-thick solgel on Kapton foil (300 μm thick) using the accelerator of ARC Seibersdorf research. The image shows single grains and clusters of grains. The substructure of clusters is visible.

8. The Commissioning Phase

The commissioning of the Rosetta spacecraft was divided into three main phases as far as the payload was concerned. The first phase was dedicated to single instrument operations. The following two phases, interference campaign and pointing campaign, investigated cross talk among the instruments or was used for calibration purposes, respectively. MIDAS participated in all three phases, however using the pointing campaign to collect measurements of the mechanical noise environment on the spacecraft rather than calibration data. Due to its mechanical complexity MIDAS exploits four launch lock mechanisms. Other movable elements were put into a passive location before launch and had to be moved mechanically into a nominal working position. The following operations were performed during the first initialization sequence of the instrument:

- Basic electronic checkout (switch on);
- Opening of the external cover by a pyro-electrical device;
- Open and close of the shutter mechanism;
- Rotation of the dust collector wheel;

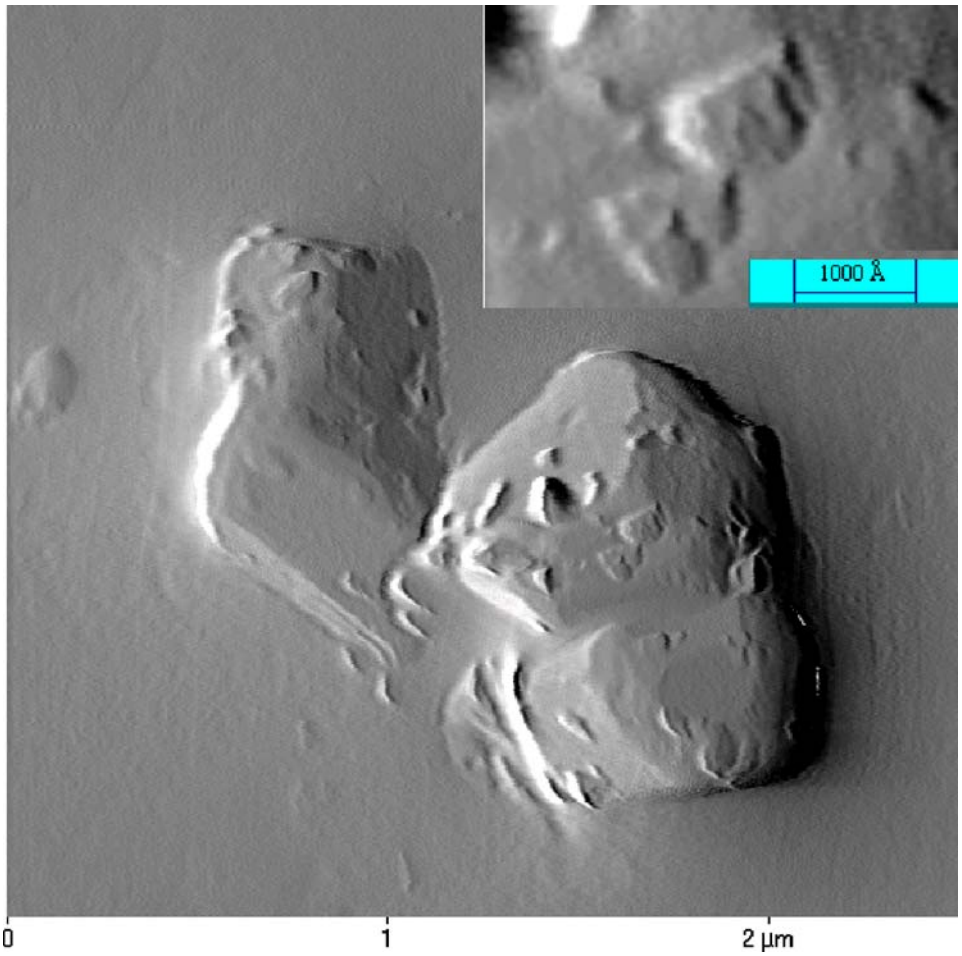

Figure 13. High-resolution image of a small cluster of Al_2N_3 grains on the collector surface. The inset shows small subcrystals from the central grain.

- Resonance search of all 16 cantilevers;
- Release of launch-locks of XYZ scanning stage (2 lock mechanisms);
- Release of base plate launch lock mechanisms (2) to activate the passive suspension system;
- Release of the approach mechanism out of the secured parking position;
- Verification of XYZ scanner by superior control loop.

These initial operations brought the instrument into a condition in which actual measurements on internal calibration samples could be performed. In addition the first check-up demonstrated the overall functionality of the instrument after launch. The resonance curves obtained for each of the 16 cantilever show no significant

deviation from the calibration measurements made during pre-tests under vacuum conditions on ground. The only detected discrepancy between predicted and measured performance concerns one of the capacitive sensors (X scanner). Connected to the X and Y scanner the capacitive sensors build a superior control loop for the scanner movement. The affected capacitive sensor provides a readout value that cannot be used for corrective measures. Since these values are used as an additional verification tool the overall system keeps the full functionality with full scientific return despite the loss of one sensor.

In the following the full procedure to make high-resolution images was applied and successfully conducted. Three different calibration samples are pre-mounted on the dust collector wheel. These etched structure are a custom sized off-spin of a commercially available product by MikroMasch EESTI (Tallinn, Estonia). The samples TGX01, TGZ02 and TGT01 are used for calibration in X-Y direction, in Z direction and for self tip imaging respectively. Several images of the XY calibration sample have been taken during commissioning. In one case, two 3×3 μm-size images of the same sample location but in two orthogonal scan directions were taken. The amplitude of the height variation was found to be 844 and 856 nm, respectively. These data confirm a high reproducibility of a collected data set between two timely separated images. The height values have not been re-calibrated yet but appear to be correct within a limit of 10 percent. The electrical and mechanical noise environment was very benign. In Table II the MIDAS main characteristics and results of the in-flight calibration campaign during the commissioning phase of the Rosetta spacecraft are listed.

A high-resolution image was acquired on a dust collector facet. In Figure 14 the coated surface is visible. The image size is $7.8\ \mu\text{m} \times 1.69\ \mu\text{m}$. The elongated featured have a height in the order of 10 nm. The elongation suggests some sort

TABLE II

MIDAS capabilities and characteristics after in-flight measurements during the commissioning phase of the Rosetta spacecraft.

Maximum scan field	94×94 μm
Minimum scan field	0.97×0.97 μm
Image resolution	256×256 pixels (typ.), 512×512 pixels (max.)
Lateral resolution	variable 3.8 nm . . . 400 nm, depending on scan field
Height resolution	0.16 nm
Number of AFM tips	16
Number of individually exposed targets	61
Number of scan areas per target	$\geq$36
Mass	8.2 kg
Power consumption	8.3 to 13.4 W (peak power $<$17 W)
Telemetry rate	100 bit s^{-1}

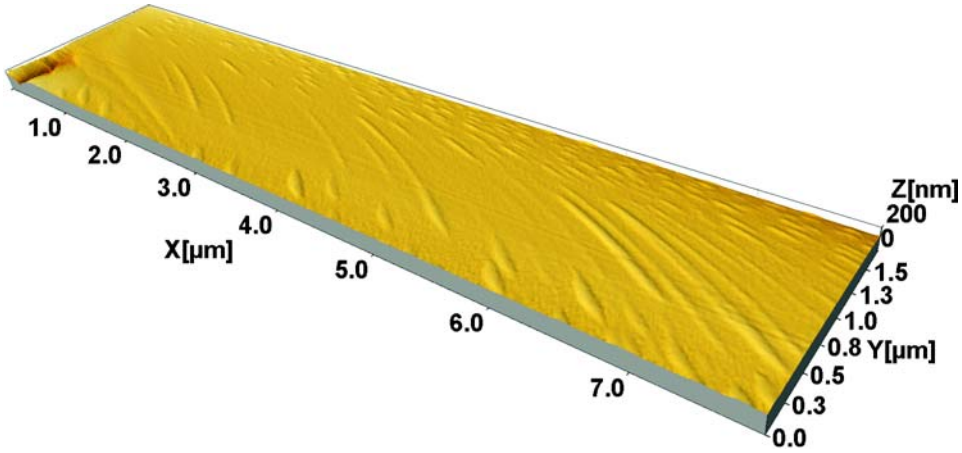

Figure 14. An image of a dust collector surface. The height of the elongated ripples is in the order of 10 nm.

of distortion. Since during the commissioning phase no sufficient warm-up can be achieved, thermal drift acting on the cantilever/piezoelectric actuator system may have contributed to these features.

9. Conclusions

The MIDAS instrument is the first application of an AFM on a space mission for in-situ planetary exploration. The basic components of the instrument set up comprise the dust collector unit, the microscope, a passive silicon rubber suspension system and an independent electronics for data acquisition, data processing and interface to the spacecraft on-board controller. The unique dust environment around a comet enables the instrument to collect solid particles while orbiting the nucleus without the requirement to actually land on the surface. The dust collection is an actively controlled process. Throughout the whole mission duration particles ejected from active regions on the comet and during different stages of cometary activity while approaching the Sun can be collected. The grain size distribution in the dust coma deduced from remote observations, earlier fly-by space missions and collected interplanetary dust particles with cometary origin suits ideally the working range of atomic force microscopy from a few micrometer down to the sub-nanometer domain.

The instrument provides textural and statistical information on the collected dust particles. In particular it will analyse the following properties:

(1) Collection of 3D images of single particles and particles aggregates at a spatial resolution of $\sim$1 nm perpendicular and $\sim$4 nm parallel to the collection surface.

At that resolution the smallest components can be identified. A distinction between solid and textural complex particles can be obtained including the identification of crystalline material if crystal faces were developed. On distinct sample surfaces sub-features like twinning defects or dissolution marks may be visible.

(2) Statistical values can be deduced from the data set. This comprises the evaluation of size, volume and shape and the variation of particle fluxes between individual exposure sequences on time scales of hours.

(3) Four out of the sixteen sensors are capable to detect a magnetic gradient between sensor and sample and allow the identification of ferromagnetic minerals or the visualisation of the internal magnetic structure of a grain. This specific mode has not been demonstrated on the flight-model yet.

The MIDAS data set will complement and form a framework for the measurements by other onboard dust analysing instruments. The capabilities of the instrument are well suited to resolve the still existing uncertainties about the structure, composition, size distribution, and temporal evolution of the cometary dust environment. Studying the properties of cometary dust with such an innovative device represents a major challenge for cometary science.

Acknowledgments

The authors herewith gratefully acknowledge the work of many engineers and technicians from the institutions involved in MIDAS. MIDAS became possible through generous support from funding agencies including the European Space Agency PRODEX programme, the Austrian Space Agency, the Austrian Academy of Sciences, ESTEC, and the German funding agency DARA (later DLR).

References

Agarwal, J., Müller, M., and Grün, E.: 2004, in: L. Colangeli *et al*. (eds.), *The New ROSETTA Targets*, Kluwer Academic Publishers, pp. 143–152.

A'Hearn, M. F., Belton, M. J. S., Delamere, *et al*.: 2005, *Science* **310**, 258.

Bradley, J. P.: 1988, *Geochem. Cosmochem. Acta* **52**, 889.

Bradley, J. P., Brownlee, D. E., and Veblen, D. R.: 1983, *Nature* **301**, 473.

Bradley, J. P., Keller, L. P., Snow, T. P., Hanner, M. S., Flynn, G. J., Gezo, J. C., *et al*.: 1999, *Science* **285**, 1716.

Clark, B. C., Green, S. F., Economou, T. E., Sandford, S. A., Zolensky, M. E., McBride, N., *et al*.: 2004, *J. Geophys. Res.* **109**, E12S03, 1.

Colangeli, L., Bar-Nun, A., Brucato, J. R., Hudson, R.L., and Moore, M.: 2004, in: M. Festou, H. U. Keller, and H. A. Weaver (eds.), *Comets II*, University of Arizona Press, Tucson, pp. 695–717.

Crovisier, J., Leech, K., Bockel, D., Morvan, E., Brooke, T. Y., Hanner, M. S., *et al*.: 1997, *Science* **275**, 1904.

Crovisier, J., Bockelée-Morvan, D., Colom, P., Biver, N., Despois, D., and Lis, D.C.: 2004, *Astron. Astrophys.* **418**, 1141.
Di Sanctis, M. C., Capria, M. T., and Coradini, A.: 2005, *Astron. Astrophys.* **444**, 605.
Ehrenfreund, P., Charnley, S. B., and Wooden, D. H.: 2004, in: M. Festou, H. U. Keller, and H. Weaver (eds.), *Comets II*, University Arizona Press, Tucson, pp. 115–133.
Fomenkova, M. N. and Chang, S.: 1993, *LPS* **XXIV**, 501.
Fomenkova, M. N. and Chang, S.: 1996, in: J. M. Greenberg (ed.), *The Cosmic Dust Connection*, Kluwer Academic Publishers, pp. 459–465.
Fomenkova, M. N. and Mendis, D. A.: 1992, *Astrophys. Space Sci.* **189**, 327.
Fulle, M., Levasseur-Regourd, A. C., McBride, N., and Hadamcik, E.: 2000, *Astron. J.* **119**, 1968.
Greenberg, J. M.: 1982, in: L. L. Wilkening (ed.), *Comets*, University of Arizona Press, pp. 131–163.
Greenberg, J. M.: 1998, *Astron. Astrophys.* **330**, 375.
Grün, E. and 25 Co-authors: 1991, in: R. L. Newburn, *et al.* (eds.), *Comets in the Post Halley Era*, Vol. 1, Kluwer Academic Publishers, pp. 277–298.
Hallenbeck, S. L., Nuth, J. A. III, and Nelson, R. N.: 2000, *Astrophys. J.* **535**, 247.
Hanner, M. S. and Bradley, J. P.: 2004, in: M. Festou, H. U. Keller, and H. A. Weaver (eds.), *Comets II*, University of Arizona Press, Tucson, pp. 555–564.
Harker, D. E. and Desch, S.: 2002, *Astrophys. J.* **565**, L109.
Harker, D. E., Woodward, C. E., Wooden, D. H., Witteborn, F. C., and Butner, H. M.: 1998, *Am. Astron. Soc. Meet.* **193**, 96.05.
Hong, S. S. and Greenberg, J. M.: 1980, *Astron. Astrophys.* **88**(1–2), 194.
Irvine, W. M. and Lunine, J. I.: 2004, in: M. Festou, H. U. Keller, and H. A. Weaver (eds.), *Comets II*, University of Arizona Press, Tucson, pp. 25–31.
Jäger, C., Molster, F. J., Dorschner, J., Henning, T., Mutschke, H., and Waters, L. B. F. M.: 1998, *Astron. Astrophys.* **339**, 904.
Jessberger, E. K.: 1999, *Space Sci. Rev.* **90**, 91.
Jessberger, E. K., Christoforidis, A., and Kissel, J.: 1988, *Nature* **332**, 691.
Kolokolova, L., Hanner, M. S., Levasseur-Regourd, A. C., and Gustafson, B.: 2004, in: M. Festou, H. U. Keller, and H. A. Weaver (eds.), *Comets II*, University Arizona Press, Tucson, pp. 577–604.
Kerr, R.: 2006, *Science* **311**, 1536.
Lasue, J. and Levasseur-Regourd, A. C.: 2006, *J. Quant. Spectros. Radiat. Transfer* **100**, 220.
Lawler, M. E. and Brownlee, D. E.: 1992, *Nature* **359**, 810.
Levasseur-Regourd, A. C., Mukai, T., Lasue, J., and Okada, Y.: 2006, *Plan. Space Sci.*, in press.
Maas, D., Krueger, F. R. and Kissel, J.: 1989, in: *Asteroids, Comets, Meteors III*, pp. 389–392.
Martin, Y. and Wickramasinghe, H. K.: 1987. *Appl. Phys. Lett.* **50**, 1455.
McKeegan, K., Aleon, J., Alexander, C., Bradley, J., Brownlee, D., Burnard, P., *et al.*: 2006, *Meteorit. Planet. Sci.* **41**, A119.
Meech, K. J.: 1991, in: R. L. Newburn, *et al.* (eds.), *Comets in the Post Halley Era*, Vol. 1, Kluwer Academic Publishers, pp. 629–669.
Messenger, S., Keller, L., Stadermann, F., Walker, R., and Zinner, E.: 2003, *Science* **300**, 105.
Min, M., Hovenier, J. W., de Koter, A., Waters, L. B. F. M., and Dominik, C.: 2005, *Icarus* **179**, 158.
Müller, M., Agarwal, J., and Grün, E.: 1998, *An Engineering Model of the Dust Environment of the Inner Coma of Comet P/Wirtanen*, RO–ESC–TA–5501, Issue 1.
Prialnik, D., Benkhoff, J., and Podolak, M.: 2004, in: M. Festou, H. U. Keller, and H. A. Weaver (eds.), *Comets II*, University of Arizona Press, Tucson, pp. 359–387.
Riedler, W., Torkar, K., Rüdenauer, F., Fehringer, M., Schmidt, R., Arends, H., *et al.*: 1998, *Adv. Space Res.* **21**(11), 1547.
Rodgers, S. D. and Charnley, S. B.: 2004, in: M. Festou, H. U. Keller, and H. A. Weaver (eds.), *Comets II*, University of Arizona Press, Tucson, pp. 505–522.

Rüdenauer, F.: 1998, *Exposure Strategies for MIDAS*; Internal Report, Austrian Research Centres Seibersdorf.
Schleicher, D.: 2006, *Icarus* **181**, 442.
Schulz, R., Stüwe, J. A., and Boehnhardt, H.: 2004, *Astron. Astrophys.* **422**, L19.
Schulze, H., Kissel, J., and Jessberger, E. K.: 1997, in: Y. J. Pendelton and A. G. G. M. Thielens (eds.), *From Stardust to Planetesimals*. ASP Conference Series 122, pp. 397–414.
Weiler, M., Knollenberg, J., and Rauer, H., in: L. Colangeli *et al*. (eds.), *The New ROSETTA Targets*, Kluwer Academic Publishers, pp. 37–46.
Wooden, D.: 2002, *Earth, Moon, and Planets* **89**(1), 247.
Zolensky, M., Bland, P., Bradley, J., Brearley, A., Brennan, S., Bridges, J., *et al*.: 2006, *Meteorit. Planet. Sci.* **41**, A167.